Main field and secular variation candidate models for the 12th IGRF generation after 10 months of Swarm measurements

Diana Saturnino, Benoit Langlais, François Civet, Erwan Thebault, Mioara Mandea

Saturnino *et al. Earth, Planets and Space* (2015) 67:96
DOI 10.1186/s40623-015-0262-7

Earth, Planets and Space
a SpringerOpen Journal

LETTER Open Access

Main field and secular variation candidate models for the 12th IGRF generation after 10 months of Swarm measurements

Diana Saturnino[1*], Benoit Langlais[1], François Civet[1], Erwan Thébault[1] and Mioara Mandea[2]

Abstract

We describe the main field and secular variation candidate models for the 12th generation of the International Geomagnetic Reference Field model. These two models are derived from the same parent model, in which the main field is extrapolated to epoch 2015.0 using its associated secular variation. The parent model is exclusively based on measurements acquired by the European Space Agency Swarm mission between its launch on 11/22/2013 and 09/18/2014. It is computed up to spherical harmonic degree and order 25 for the main field, 13 for the secular variation, and 2 for the external field. A selection on local time rather than on true illumination of the spacecraft was chosen in order to keep more measurements. Data selection based on geomagnetic indices was used to minimize the external field contributions. Measurements were screened and outliers were carefully removed. The model uses magnetic field intensity measurements at all latitudes and magnetic field vector measurements equatorward of 50° absolute quasi-dipole magnetic latitude. A second model using only the vertical component of the measured magnetic field and the total intensity was computed. This companion model offers a slightly better fit to the measurements. These two models are compared and discussed.We discuss in particular the quality of the model which does not use the full vector measurements and underline that this approach may be used when only partial directional information is known. The candidate models and their associated companion models are retrospectively compared to the adopted IGRF which allows us to criticize our own choices.

Keywords: Magnetic field; Main field; Secular variation; Modeling; IGRF; Time extrapolation

Findings

Introduction

The International Geomagnetic Reference Field (IGRF) is a time series of Main Field (MF) Spherical Harmonic (SH) Gauss coefficients aiming to describe the large-scale Earth's magnetic field of internal origin, also known as the main field. It is published every 5 years and includes a predictive Secular Variation (SV) part for the next 5-year period. IGRF models result from a collective and international effort, in order to derive the most accurate model of the main geomagnetic field at a given epoch.

Since the ninth generation of IGRF (Macmillan et al. 2003) Gauss coefficients are computed up to SH degree and order 13 for the static part and up to SH degree and order 8 for the secular variation part. All coefficients are rounded at 0.1 nT or 0.1 nT.yr^{-1}, respectively.

The latest 12th generation of the IGRF model comes almost 1 year after the successful launch of the ESA three-satellite Swarm mission on 22 November 2013. A full presentation of the mission and of some of its expected outputs can be found in Olsen et al. (2013), Chulliat et al. (2013), and Thébault et al. (2013). After an initial stage where all three satellites flew around 495 km, two satellites fly almost side-by-side at a nominal altitude close to 465 km, while the third one flies some 50 km higher. All three are on near polar orbits. Each satellite carries two magnetic field instruments on a boom. The first one is the Vector Fluxgate Magnetometer (VFM) and is co-mounted on an optical bench with the Star TRacker (STR) with three Camera Head Units (CHUs) to determine the attitude of the spacecraft. This is necessary to transform the vector readings into geocentric B_X, B_Y, and B_Z magnetic

*Correspondence: diana.saturnino@univ-nantes.fr
[1] Laboratoire de Planétologie et Géodynamique de Nantes, UMR 6112 CNRS, Université de Nantes, Nantes, France
Full list of author information is available at the end of the article

field components (horizontal northward, horizontal eastward, and vertical downward, respectively). The second one is the Absolute Scalar Magnetometer (ASM) and aims at providing very accurate 1 Hz absolute scalar measurements F for both scientific and VFM calibration purposes.

Our candidate model exclusively relies on the measurements made by the low-altitude Swarm A and C spacecrafts. In the following, we describe the data selection scheme. Because some discrepancies were observed between the scalar magnitude as computed from the VFM measurements and the ASM direct measurements, two datasets were built. In the first dataset, all VFM and ASM measurements were considered. In the second one, we disregarded the horizontal magnetic field components of the VFM measurements. These two datasets are used to derive two models, which are denoted V-ASM and Z-ASM, respectively. In the third section, we briefly describe the model parametrization, and compare and discuss the two models in "Comparison of V-ASM and Z-ASM models" section, justifying our decision to present the V-ASM model as our IGRF-12 candidate model. Finally, we retrospectively compare our models to the adopted IGRF-12 model, which allows us to underline the shortcomings of the chosen approach.

Data selection

Our models are based on Swarm A and C satellite measurements. This facilitates the identification of outliers as these satellites fly side-by-side. Whenever appropriate, the priority is given to versions RPRO301, OPER302, and OPER301 of the processed measurements. The following flags (Tøffner-Clausen 2013), although provisional, are used:

- `flags_B`: 0 or 1 (VFM is nominal or ASM is turned off);
- `flags_F`: 0 or 1 (ASM is nominal or running in vector mode);
- `flags_q`: between 0 and 6, or between 16 and 22 (at least two CHUs nominal);
- `flags_Platform`: 0 or 1 (nominal telemetry or thrusters not activated).

We then select measurements according to several parameters to reduce the importance of external fields. The Dst and Kp indices are used, as well as a local time selection:

- $-5 \leq \mathrm{Dst} \leq 5$ nT for the considered time;
- $|\ \mathrm{dDst/dt}\ | \leq 3\ \mathrm{nT.h}^{-1}$;
- $0^0 \leq \mathrm{Kp} \leq 1^+$;
- $\mathrm{Kp} \leq 2^-$ for the previous and following 3-h time intervals;
- local time between 20:00 and 4:00.

This latter selection criterion is preferred over a more strict one based on the illumination of the spacecraft. This would result in large gaps over polar areas during the summer of each hemisphere (Lesur et al. 2010). VFM and ASM measurements are used within $\pm$ 50° quasi-dipole magnetic latitude, while only scalar measurements by the ASM are considered in the polar areas. Known differences exist between intensity F measurements by the ASM and intensity B computed from VFM measurements, with a root mean square (rms) difference of the order of 1 nT. At the time of deriving the model, no official and definitive strategy has been defined, so we do not take these differences into account and do not scale VFM intensity to match ASM measurements. Instead, we overcome this problem by building two datasets. Both use intensity measurements, but while the first one is completed by full vector measurements, in the second one, we consider only the vertical component of the measurements. This means that the second dataset and associated model depend more moderately on these calibration issues.

In a preliminary stage, we also check data for possible outliers, by looking for possible large discrepancies between observations and predictions by a first version of our model. We chose to eliminate all data acquired on the days when such large discrepencies were observed (year–day of year): 2013352 (VFM), 2014084 (ASM and VFM), 2014085 (ASM and VFM), 2014098 (ASM and VFM), 2014099 (ASM and VFM), 2014181 (ASM), 2014182 (ASM), 2014185 (ASM), 2014188 (ASM). Only Swarm C measurements were eliminated in this step. We however note that this selection came only after data selection with respect to flags and indices. In the last stage of our approach, we further reject measurements associated with large residuals, exceeding 15 nT for B_Z, 25 nT for B_X or B_Y for the VFM, and 35 nT for the ASM (these arbitrary values are about five times the final rms difference). This corresponds to remove about 1 % of ASM measurements and 0.2 % of the VFM triplets.

Finally, data are decimated along tracks. Only one measurement every 15 days is kept, corresponding to a spacing of about 100 km along orbit. Data distribution is homogenized, keeping a maximum of three data points per $6 \times 6°$ bins per 15-day intervals. The resulting geographic and time data distributions are shown in Figs. 1 and 2, respectively. The local time drift of the spacecraft results in no vector triplets during two periods, at the beginning of the northern spring and at the end of the southern winter. During these two periods, the only data fulfilling our selection criteria are ASM measurements very close to the pole, i.e., where fast local time variations occur. This means that these measurements may be on the day side and above

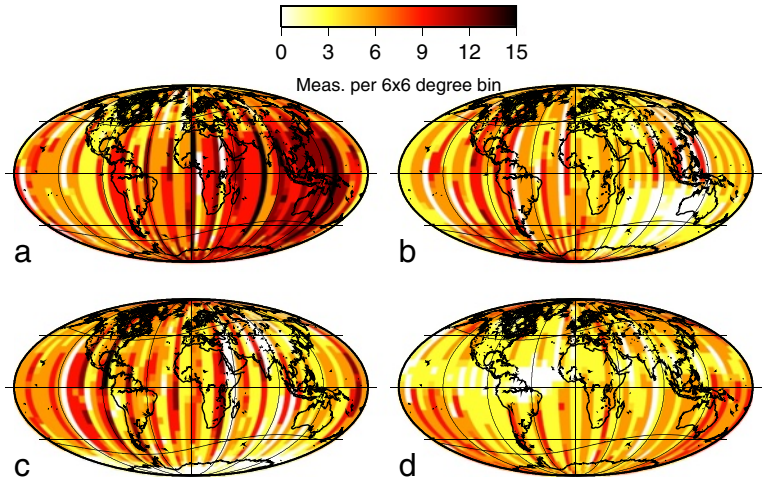

Fig. 1 Number of measurements per 6 × 6° bin, centered on the winter solstice (**a**), spring equinox (**b**), summer solstice (**c**), and autumn equinox (**d**)

the sun horizon, this is especially true for the measurements above the northern hemisphere in June and July.

Model parametrization and statistics

While IGRF MF and SV models are published up to SH degree and order 13 and 8, respectively, we computed parent models to higher degree to avoid possible aliasing (e.g., Whaler 1986). The static part of the internal field, described by g_n^m, h_n^m Gauss coefficients of degree n and order m, is computed up to SH degree 25 and the secular variation up to 13. Given the short time interval covered by the data (10 months), we assume a constant secular variation and do not consider secular acceleration. The external magnetic field is described by q_n^m, s_n^m Gauss coefficients. It is computed up to SH degree 2. A linear dependence with respect to the Dst index for the first degree is also considered with $q_n^{\tilde{m}}$ and $s_n^{\tilde{m}}$, with internal induced counterpart represented by Q_1. Internal and external magnetic potentials at spherical

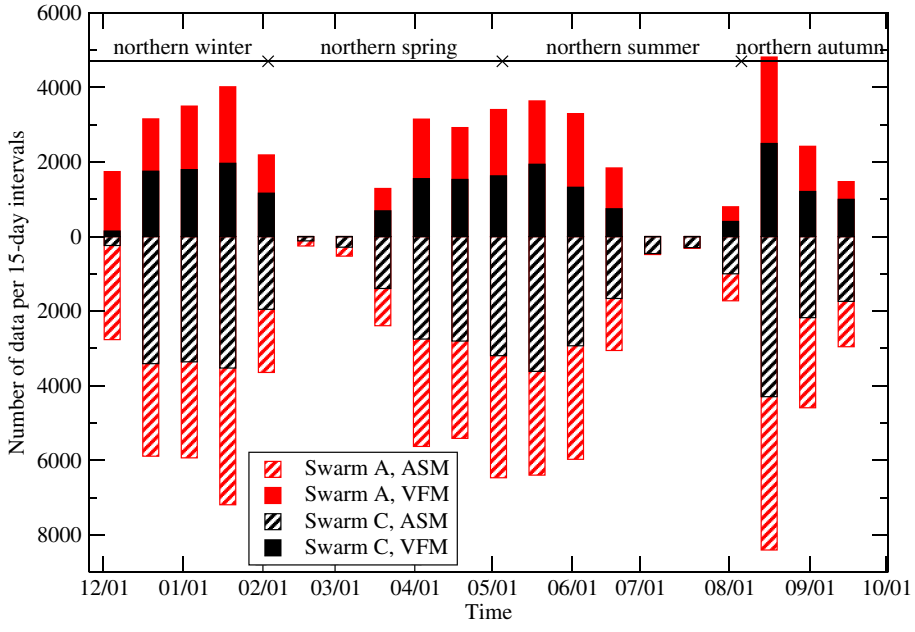

Fig. 2 Time distribution for Swarm A and Swarm C ASM and VFM measurements, per 15-day intervals. Seasons are indicated for comparison with Fig. 1

coordinates (r, θ, ϕ) are written as (e.g., Langlais et al. 2003):

$$V_{\text{int}}(r,\theta,\phi,t) = a\sum_{n=1}^{25}\left(\frac{a}{r}\right)^{n+1}\sum_{m=0}^{n}\left(g_n^m(t)\cos(m\phi) + h_n^m(t)\sin(m\phi)\right)P_n^m(\cos(\theta)) \quad (1)$$

$$\begin{aligned} V_{\text{ext}}(r,\theta,\phi,t) = {} & a\sum_{n=1}^{2}\left(\frac{r}{a}\right)^{n}\sum_{m=0}^{n}\left(q_n^m\cos(m\phi) + s_n^m\sin(m\phi)\right)P_n^m(\cos(\theta)) \\ & + Dst\sum_{n=1}^{1}\left[\left(\frac{r}{a}\right)^{n} + Q_1\left(\frac{a}{r}\right)^{n+1}\right] \\ & \times\sum_{m=0}^{n}\left(\tilde{q_n^m}\cos(m\phi) + \tilde{s_n^m}\sin(m\phi)\right)P_n^m(\cos(\theta)) \end{aligned} \quad (2)$$

where a is the Earth's reference radius (6371.2 km) and Q_1 is set to 0.27 (Langel and Estes 1985). The inverse problem is linearized and solved using a least square method (Cain et al. 1989). The choice of the initial model has no effect on the final result as long as it is close enough to the actual field, such as a model at a different epoch (e.g., Langlais et al. 2003). Convergence was reached after two iterations.

There are 881 coefficients to solve, using 38,437 Swarm A ASM scalar measurements, 22,320 Swarm A VFM vector triplets, 40,609 Swarm C ASM scalar measurements, and 21,292 Swarm C VFM vector triplets. The mean epoch of measurements is 2014.3. To overcome the denser data distribution close to the poles, we used a $1/\sin\theta$ weighting scheme (with θ being the colatitude). In the first model, we observed that the misfit for Swarm C was slightly larger than for Swarm A. Because both satellites essentially measure the same magnetic field, they should be associated with similar errors. We therefore chose to give more importance to the latter, with a 9/8 ratio, and weighted the data accordingly.

We give in Table 1 the statistics of the derived model, denoted V-ASM. As mentioned, the misfit associated with Swarm C measurements is slightly worse than that associated with the Swarm A measurements, with a 9/8 ratio (corresponding to the different weights allocated to both satellites). This is particularly true for the B_Y component, for which both the rms and the mean differences are 14 and 100 % larger, respectively. This fact, combined to the slight differences between the ASM scalar reading of the magnetic field intensity and the one computed from the VFM measurements, led us to explore an alternative modeling strategy.

It is not possible to model the Earth's magnetic field using only scalar measurements without any prior because of the so-called Backus effect. This effect comes from the non-uniqueness of the inverse problem and is characterized by focused large errors perpendicular to the measured field. This occurs mostly in the equatorial region, and it results in large differences in the vertical component. This effect was discovered and described when no spacecraft vector magnetic field measurements were available (e.g., Backus 1970; Hurwitz and Knapp 1974; Lowes 1975; Stern and Bredekamp 1975). Different strategies have been proposed to alleviate it. Hurwitz and Knapp (1974) were probably the first to include vector data in the equatorial region, to better constrain the position of the magnetic equator and resolve the sectoral harmonics. These additional data can be provided by the magnetic observatories, which have however a poor geographic distribution. Additional information can also be obtained from a triaxial magnetometer on board a satellite, which requires an accurate determination of the satellite attitude (Holme 2000; Holme and Bloxham 1995). Indeed, (Khokhlov et al. 1997, 1999) showed that it is possible to eliminate the Backus effect if the position of the geomagnetic equator (where $B_Z = 0$) is known. This position can be directly estimated by a time extrapolation from a previous or later epoch model (Ultré-Guérard et al. 1998a,b) or indirectly from measurements of the equatorial electrojet (Holme et al. 2005).

An approach similar to that of Ultré-Guérard et al. (1998a) was already employed in the context of IGRF modeling, but this was to test the quality of the candidate models rather than to propose a new model (Mandea and Langlais 2000). Here, we combine direct measurements of the position of the geomagnetic equator (i.e., vertical field measurements) to scalar measurements. The new model will not depend on the possibly more perturbed

Table 1 Root mean square and mean differences (in nT) for the two parent models and for Swarm A and C. The *B* misfit corresponds to intensity rms difference computed from the VFM dataset. *F* misfits are sorted with respect to the magnetic absolute latitude 50°

		Root mean square difference						Mean difference					
Model	Sat.	B_X	B_Y	B_Z	B	$F_{\leq 50}$	$F_{>50}$	B_X	B_Y	B_Z	B	$F_{\leq 50}$	$F_{>50}$
V-ASM	A	4.10	3.94	2.71	3.05	3.07	8.93	0.12	0.72	0.16	−0.09	0.01	−0.46
V-ASM	C	4.19	4.49	3.10	3.03	3.11	9.31	0.32	1.41	−0.07	0.19	0.18	−0.26
Z-ASM	A	4.38	4.14	2.51	3.04	3.05	8.91	0.58	0.74	0.23	−0.03	0.04	−0.14
Z-ASM	C	4.46	4.72	2.88	3.02	3.09	9.29	0.80	1.49	−0.04	−0.33	0.01	0.20

Table 2 Root mean square differences at the surface of the Earth (in nT) between the candidate models for different truncation degrees and different epochs. In the last row, only the SV is considered (in nT.yr^{-1})

Model 1	Model 2	Epoch	Degree	B_X	B_Y	B_Z	B
V-ASM	Z-ASM	2014.3	25	1.39	1.81	1.90	1.48
V-ASM	Z-ASM	2014.3	13	0.72	0.68	1.13	0.94
V-ASM	Z-ASM	2015.0	25	2.71	2.34	3.67	3.26
V-ASM	Z-ASM	2015.0	13	2.46	1.62	3.36	3.04
IGRF-12	V-ASM	2015.0	13	6.40	5.50	9.22	9.30
IGRF-12	Z-ASM	2015.0	13	6.77	5.87	9.77	9.90
V-ASM	Z-ASM	2015.0	8 (SV)	2.64	1.65	3.59	2.98

horizontal components (Table 1), and mismatch between B and F (below 50° absolute magnetic latitude) should not introduce any intrinsic error. This latter point is however debatable, as even the intensity of the measured vertical field depends on the measured F ASM value through the calibration process.

We give in Table 1 the statistics of this second model, denoted Z-ASM, derived using the second dataset. The rms difference for the B_Z component is improved, with a decrease of about 7 % for both satellites with respect to the V-ASM model. The misfit for F and B also display a slight decrease with respect to the V-ASM model. On the contrary, the rms differences for horizontal components and for both satellites are degraded, in a similar proportion than for the B_Z improvement. The mean deviation for B_X difference changes significantly from the V-ASM to the Z-ASM model, with an increase of 0.5 nT for both Swarm A and C datasets. A similar change is also observed for F in polar areas.

Comparison of V-ASM and Z-ASM models

We now compare our two models at the Earth's reference radius. We present in Table 2 rms differences between the models, for two different epochs (the mean epoch at 2014.3 and the reference epoch at 2015.0) and for the full expansion (i.e., $N^{\max} = 25$) or that truncated to SH degree and order 13 (corresponding to the IGRF candidate model). Our two models are very similar at their mean time, with differences of the order of 1.5 to 2 nT, for the full spherical harmonic expansion. These differences increase by a factor of 2 (except for B_Y) when both models are extrapolated to epoch 2015.0 (third row of Table 2) and decrease slightly when the models are truncated to degree 13 for the main field (fourth row).

The geographic distribution of the differences between V-ASM and Z-ASM truncated models is presented in Figs. 3 and 4 at their mean epoch and at 2015.0, respectively. These differences are dominated by both small scales (longitudinal B_Y and B_Z differences) and an almost dipolar pattern (East-West for B_Y and North-South for B_Z). This is confirmed when examining the differences coefficient by coefficient. We show in Fig. 5 these differences up to SH degree 13. The largest difference is 0.48 nT (for g_1^1), and it exceeds 0.1 nT for only 16 coefficients. Beyond SH degree 13, noticeable differences, between 0.1 and 0.2 nT, are only found for degree 15, 16,

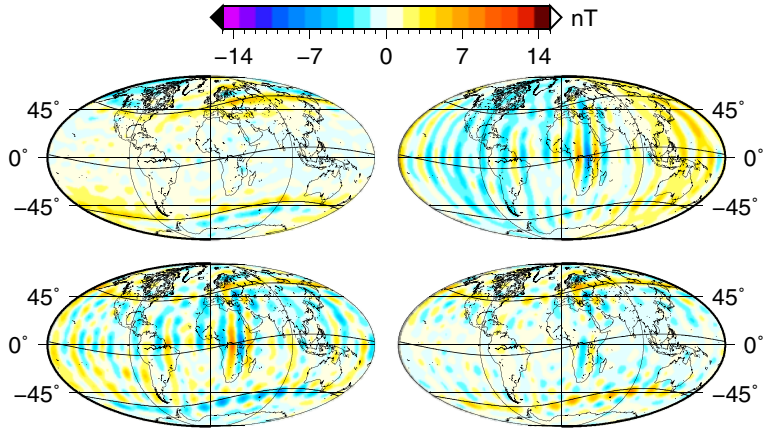

Fig. 3 Difference at Earth's mean radius between V-ASM and Z-ASM models at epoch 2014.3 and for the full expansion. From *top left* to *bottom right*, B_X, B_Y, B_Z, and B, respectively. Thin lines indicate magnetic equator and 50° magnetic quasi-dipole latitudes

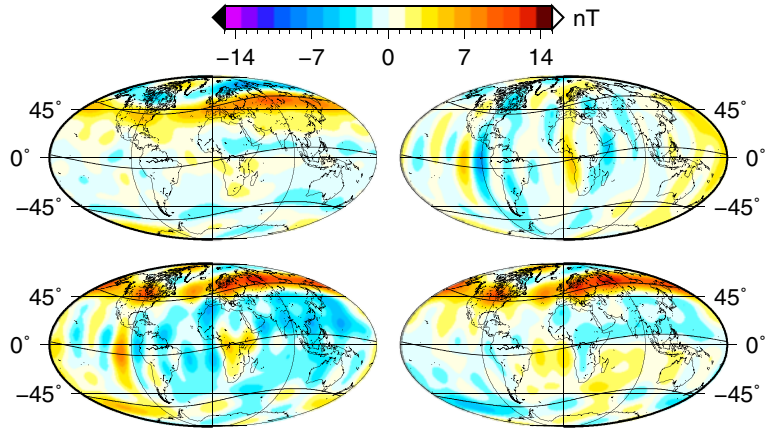

Fig. 4 Same as Fig. 3 between V-ASM and Z-ASM models at epoch 2015.0 and truncated to $n = 13$

and 17 sectoral coefficients (not shown). Together with those of the inclined dipole, they explain the geographic differences seen in Fig. 3. There are also some differences which coincide with the ±50° magnetic latitude data separation into scalar only and scalar plus vector measurements. These differences are moderate at the mean epoch of measurements, but they increase when the model is extrapolated to 2015.0, as seen in Fig. 4. Above northern Europe, the two models differ by more than 10 nT, except for B_Y. The difference is less important in the southern hemisphere.

When comparing the two SV models truncated at degree 8 (Fig. 6 and Table 2), we obtain differences with similar geographical patterns and comparable intensity values as for the MF model comparison. The coefficient comparison is shown in Fig. 7. The largest difference is 1.47 nT.yr^{-1} for g_2^0. The 11 coefficients with largest differences explain almost 90 % of total difference (2.54 versus 2.98 nT.yr^{-1} rms differences for the full model for B, with a correlation coefficient of 0.8 between the full model and that based on these 11 coefficients only).

We finally compare the spectra of the different models, which are presented in Fig. 8 at epoch 2015.0. Both V-ASM and Z-ASM MF models are very similar, and their differences do not exceed 4 nT^2 per degree. The differences between the two SV models are slightly larger, up to 8 nT^2.yr^{-2} per degree. Both V-ASM and Z-ASM models display larger energy in their secular variation spectra

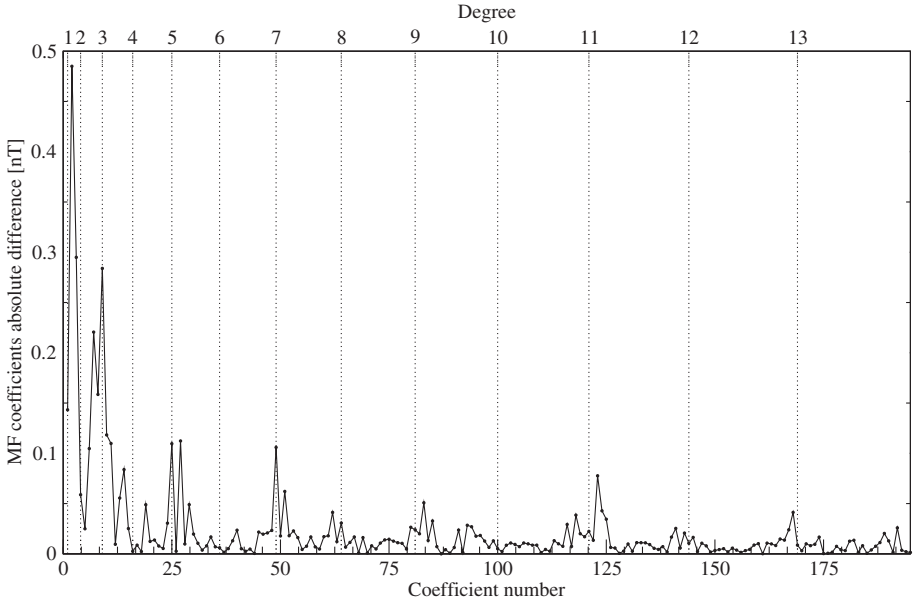

Fig. 5 Absolute difference of Gauss coefficients between V-ASM and Z-ASM models up to 13 at epoch 2015.0

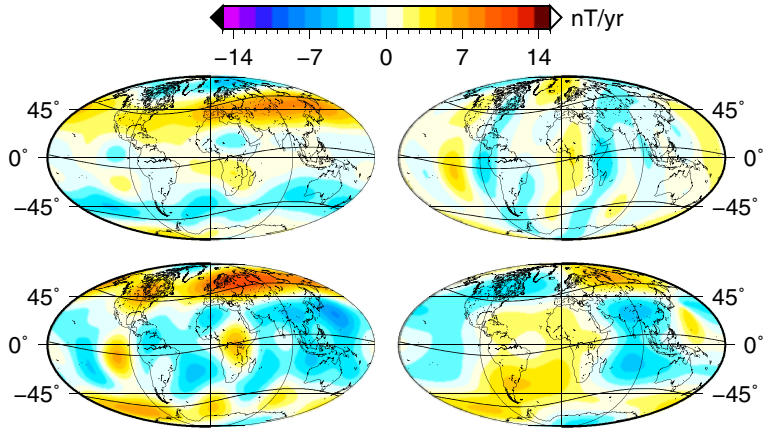

Fig. 6 Same as Fig. 3 between V-ASM and Z-ASM secular variation models at epoch 2015.0 and truncated to $n = 8$

for degree 10 and 12 terms, with the Z-ASM model being 50 % more energetic than the V-ASM model for these two terms. Although these SV coefficients are not directly included in the SV candidate model for IGRF, these may affect our MF candidate model when it is extrapolated to epoch 2015.0, and this is the reason why we eventually decided to present truncated versions of the V-ASM (MF and SV) model for IGRF candidate models. We nonetheless observe that the spectrum of our candidate model is probably too energetic for its SV part at SH degrees 7 and 8. It is likely that the SV is not constrained enough when using less than 1 year of measurements (e.g., Barraclough 1985; Langlais et al. 2003).

Comparison with the IGRF-12 model

We now compare our candidate and our test models (which are truncated and extrapolated versions of the V-ASM and Z-ASM parent models, respectively) to the adopted 12th IGRF generation. This a posteriori comparison is only possible because IGRF was adopted between the time at which we computed our candidate models and the time at which this study is written (Thébault et al. 2015b). Note that IGRF models depend, among others, on our candidate models.

Statistics are given in Table 2. We also show geographic differences between IGRF and our candidate models in Fig. 9 and compare the different spectra in Fig. 8. A more

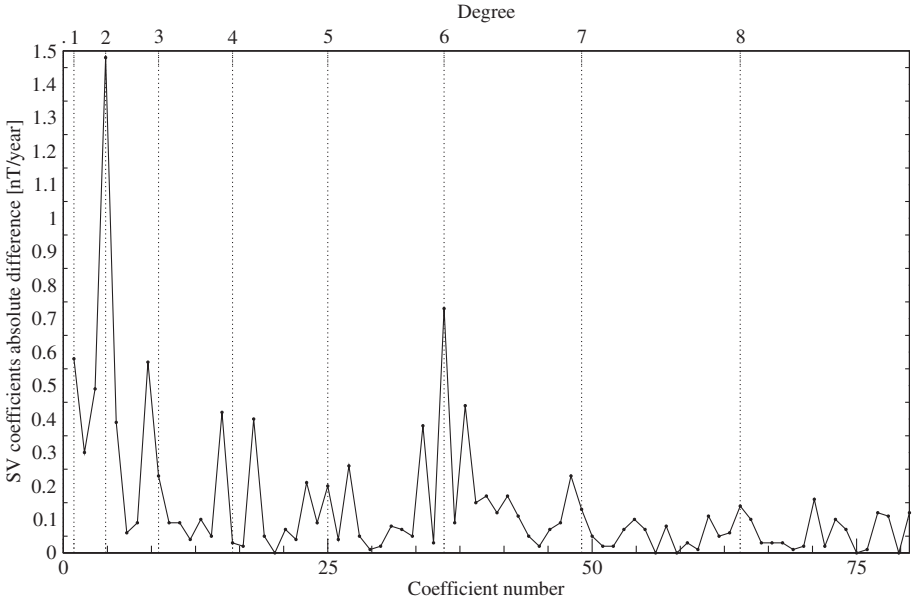

Fig. 7 Absolute difference of Gauss coefficients between V-ASM and Z-ASM SV models up to degree 8 at epoch 2015.0

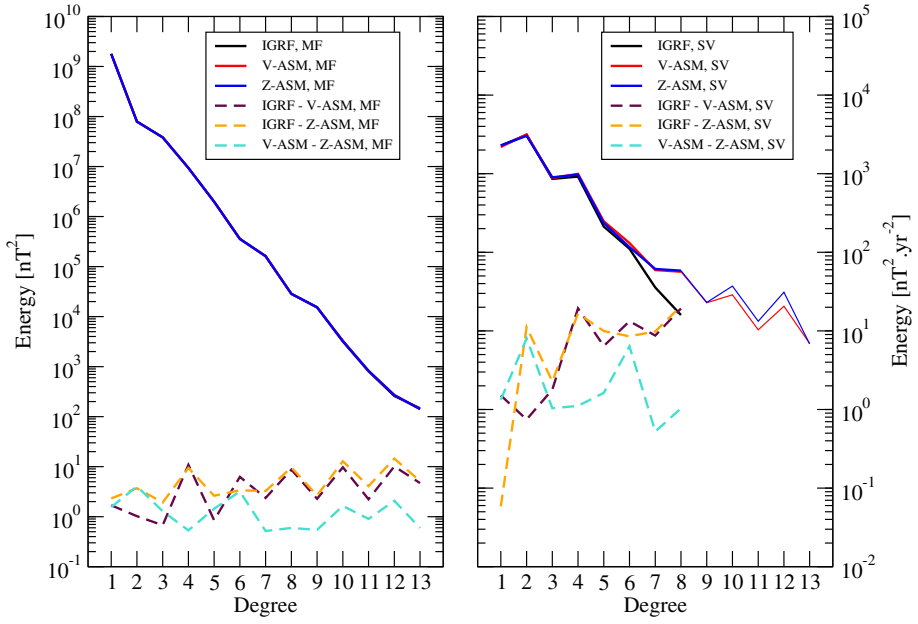

Fig. 8 Magnetic energy spectra of V-ASM, Z-ASM, and adopted IGRF models, for the main field (*left panel*) and the secular variation (*right panel*). Also shown are the spectra of the differences between models. For the SV, models are shown up to degree 13, although terms for $n > 8$ are not considered for IGRF. Note that on the *left panel*, *red*, *black*, and *blue curves* are superimposed

complete comparison between the adopted IGRF and all other candidate models can be found in Thébault et al. (2015a). Rms differences between IGRF and our candidate model range between 6 and 10 nT for the main field depending on the field component. This is almost three times that between our two parent models. A close look at the geographic distribution of the residuals reveals that most of the differences are located poleward of 50° absolute magnetic latitude. In the equatorial region, differences range between ± 9.5 nT but may exceed ± 40 nT in polar areas. Globally, differences tend to be aligned with magnetic latitudes, this may be related to noise that correlates with magnetic latitudes such as the noise due to the ionosphere and magnetosphere. The considered time interval of 10 months is also probably too short to reliably constrain the secular variation up to degree and order 8. Nonetheless, differences between IGRF and our V-ASM-derived candidate model are slightly lower than those with our Z-ASM-derived test model, which supports our preferred choice regarding the V-ASM model.

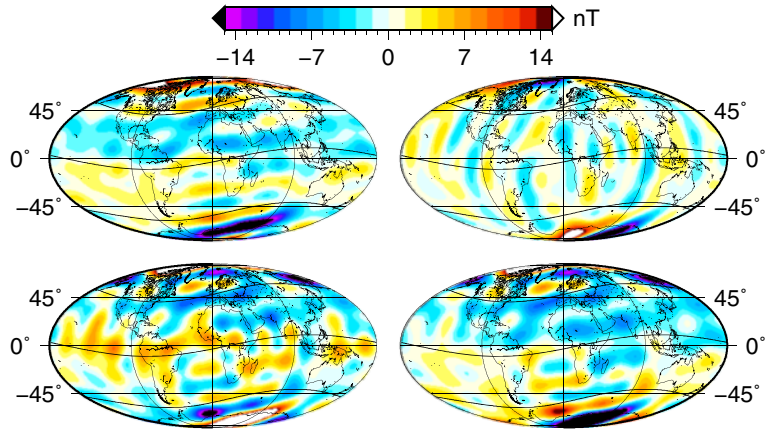

Fig. 9 Same as Fig. 3 between IGRF and V-ASM main field models at epoch 2015.0 and truncated to $n = 13$

Concluding remarks

We present two candidate models for IGRF-12 for the main field at epoch 2015.0 and for the secular variation between 2015 and 2020. We choose to compute parent models with a simple parametrization and without adding regularization or temporal splines. Only Swarm A and C measurements, acquired during the first 10 months of the mission, are considered, with external activity indices selection and outliers removal. We compare two different modeling strategies, one using full vector measurements and one using only vertical component measurements, both in addition to intensity measurements. We show that the differences between these models are small when they are compared at the mean epoch of measurements for $n \leq 13$. However, they become larger when the models are extrapolated to 2015.0, increasing from 0.94 to 3.04 nT. This is very likely a consequence of using a too short time interval to construct our SV model.

The two models are relatively similar for the static part, and only the time-varying part is different. The analysis of this difference lead us to chose the V-ASM parent model of our MF and SV candidates for IGRF. We believe that this difference is related both to a non-optimal data selection above polar areas (where the misfit is very large) and to a too short time interval to constrain the secular variation. We however want to underline that using the vertical magnetic field in complement to globally distributed scalar measurements to reduce the Backus effect is promising, and that such approach may be explored in the future if required.

Competing interests

The authors declare that they have no competing interests.

Authors' contributions

All authors contributed to the manuscript. DS and BL initiated the work. FC and ET made initial data selection and tests. All authors participated to the construction of the candidate models. All authors read and approved the final manuscript.

Acknowledgements

The authors acknowledge ESA for provided access to the Swarm L1b data. DS and FC are supported by CNES and Région Pays de la Loire. This work was partly funded by the Centre National des Études Spatiales (CNES) within the context of the "Travaux préparatoires et exploitation de la mission Swarm" project. We also thank two anonymous reviewers for their detailed comments.

Author details

[1] Laboratoire de Planétologie et Géodynamique de Nantes, UMR 6112 CNRS, Université de Nantes, Nantes, France. [2] Centre National d'Études Spatiales, Paris, France.

Received: 12 February 2015 Accepted: 3 June 2015
Published online: 20 June 2015

References

Backus G (1970) Non-uniqueness of the external geomagnetic field determined by surface intensity measurements. J Geophys Res 75:6337–6341. doi:10.1029/JA075i031p06339

Barraclough DR (1985) A comparison of satellite and observatory estimates of geomagnetic secular variation. J Geophys Res 90:2523–2526. doi:10.1029/JB090iB03p02523

Cain JC, Wang Z, Kluth C, Schmitz DR (1989) Derivation of a geomagnetic model to $n = 63$. Geophys Jour 97:431–441. doi:10.1111/j.1365-246X.1989.tb00513.x

Chulliat A, Vigneron P, Thébault E, Sirol O, Hulot G (2013) Swarm SCARF dedicated ionospheric field inversion chain. Earth Planets Space 65. doi:10.5047/eps.2013.08.00

Holme R (2000) Modeling of attitude error in vector magnetic data: application to Ørsted data. Earth Planets Space 52:1187–1197. doi:10.1186/BF03352351

Holme R, Bloxham J (1995) Alleviation of the Backus effect in geomagnetic field modelling. Geophys Res Lett 22. doi:10.1029/95GL01431

Holme R, James MA, Lühr H (2005) Magnetic field modelling from scalar-only data: resolving the Backus effect with the equatorial electrojet. Earth Planets Space 57. doi:10.1186/BF03351905

Hurwitz L, Knapp DG (1974) Inherent vector discrepancies in geomagnetic main field models based on scalar F. J Geophys Res. 79:3009–3013. doi:10.1029/JB079i020p03009

Khokhlov, A, Hulot G, Le Mouel J-L (1997) On the Backus effect-I. Geophys J Int 130. doi:10.1111/j.1365-246X.1997.tb01864.x

Khokhlov A, Hulot G, Le Mouel J-L (1999) On the Backus effect-II. Geophys J Int 137. doi:10.1046/j.1365-246X.1999.00843.x

Langel RA, Estes RH (1985) The near-Earth magnetic field at 1980 determined from MAGSAT data. J Geophys Res. 90:2495–2509. doi:10.1029/JB090iB03p02495

Langlais B, Mandea M, Ultré-Guérard P (2003) High-resolution magnetic field modeling: application to MAGSAT and Ørsted data. Phys Earth Planet Int 135:77–91. doi:10.1016/S0031-9201(02)00207-8

Lesur V, Wardinski I, Hamoudi M, Rother M (2010) The second generation of the GFZ Reference Internal Magnetic Model: GRIMM-2. Earth Planets Space 62. doi:10.5047/eps.2010.07.007

Lowes FJ (1975) Vector errors in spherical harmonic analysis of scalar data. Geophys J R Astr Soc 42:637–651. doi:10.1111/j.1365-246X.1975.tb05884.x

Macmillan S, Maus S, Bondar T, Chambodut A, Golovkov V, Holme R, Langlais B, Lesur V, Lowes F, Lühr H, Mai W, Mandea M, Olsen N, Rother M, Sabaka T, Thomson A, Wardinski I (2003) The 9th-generation International Geomagnetic Reference Field. Phys Earth Planet Int 140:253–254. doi:10.1111/j.1365-246X.2003.02102.x

Mandea M, Langlais B (2000) Use of Ørsted scalar data in evaluating the pre-Ørsted main field candidate models for the IGRF 2000. Earth Planets Space 52:1167–1170. doi:10.1186/BF03352347

Olsen N, Friis-Christensen E, Alken P, Beggan CD, Chulliat A, Doornbos E, da Encarnacao JT, Hamilton B, Hulot G, van den IJssel J, Kuvshinov A, Lesur V, Luehr H, Macmillan S, Maus S, Noja M, Olsen PEH, Park J, Plank G, Puethe C, Rauberg J, Ritter P, Rother M, Sabaka TJ, Schachtschneider R, Sirol O, Stolle C, Thébault E, Thomson AWP, Toffner-Clausen L, Velimsky J, Vigneron P, Visser PN (2013) The Swarm Satellite Constellation Application and Research Facility (SCARF) and Swarm data products. Earth Planets Space 65. doi:10.5047/eps.2013.07.00

Stern DP, Bredekamp JH (1975) Error enhancement in geomagnetic models derived from scalar data. J Geophys Res 80:1776–1782. doi:10.1029/JA080i013p01776

Thébault E, Finlay CC, Alken P, Beggan C, Canet E, Chulliat A, Langlais B, Lesur V, Lowes FJ, Manoj C, Rother M, Schachtschneider R (2015a) Evaluation of candidate geomagnetic field models for IGRF-12. Earth Planets Space. Under revision

Thébault E, Finlay CC, Beggan C, Alken P, Aubert J, Barrois O, Bertrand F, Bondar T, Boness A, Brocco L, Canet E, Chambodut A, Chulliat A, Coïsson P, Civet F, Du A, Fournier A, Fratter I, Gillet N, Hamilton B, Hamoudi M, Hulot G, Jager T, Korte M, Kuang W, Lalanne X, Langlais B, Léger J-M, Lesur V, Lowes FJ, Macmillan S, Mandea M, Manoj C, Maus S, Olsen N, Petrov V, Rother M, Sabaka TJ, Saturnino D, Schachtschneider R, Sirol O, Tangborn A, Taylor V, Thomson A, Tøffner-Clausen L, Vigneron P, Wardinski I, Zvereva T (2015b) International Geomagnetic Reference Field: the twelfth generation. Earth Planets Space. doi:10.1186/s40623-015-0228-9

Thébault E, Vigneron P, Maus S, Chulliat A, Sirol O, Hulot G (2013) Swarm SCARF dedicated lithospheric field inversion chain. Earth Planets Space 65. doi:10.5047/eps.2013.07.00

Tøffner-Clausen L (2013) Swarm level 1b product definition. Technical Report SW-RS-DSC-SY-0007, Issue 5.15. National Space Institute, Technical

University of Denmark [Available at https://earth.esa.int/documents/10174/1514862/Swarm_L1b_Product_Definition.]
Ultré-Guérard P, Hamoudi M, Hulot G (1998a) Reducing the Backus effect given some knowledge of the dip-equator. Geophys Res Lett 25. doi:10.1029/98GL02211
Ultré-Guérard P, Jault D, Alexandrescu M, Achache J (1998b) Improving geomagnetic field models for the period 1980–1999 using Ørsted data. Earth Planets Space 50:635–640
Whaler KA (1986) Geomagnetic evidence for fluid upwelling at the core-mantle boundary. Geophys J R Astr Soc 86:563–588. doi:10.1111/j.1365-246X.1986.tb03844.x